Tick extracellular vesicles impair epidermal homeostasis through immune-epithelial networks during hematophagy

Liron Marnin[1], Haikel N. Bogale[2†], Hanna J. Laukaitis-Yousey[1], Luisa M. Valencia[1], Agustin Rolandelli[1], Anya J. O'Neal[1‡], Camila Rodrigues Ferraz[1], Axel D. Schmitter-Sánchez[3,4,5], Emily Bencosme Cuevas[6], Thu-Thuy Nguyen[6], Brenda Leal-Galvan[7], David M. Rickert[1], Vincent M. Bruno[1,2], M. Tays Mendes[1§#], Sourabh Samaddar[1], L. Rainer Butler[1], Nisha Singh[1], Francy E. Cabrera Paz[1], Jonathan D. Oliver[8], Julie M Jameson[9], Ulrike G. Munderloh[10], Adela S. Oliva Chávez[7], Albert Mulenga[6], Sangbum Park[3,4,5], David Serre[1,2], and Joao H.F. Pedra[1*].

Affiliations:

[1]Department of Microbiology and Immunology, University of Maryland School of Medicine, Baltimore, MD, USA.

[2]Institute for Genome Sciences, University of Maryland School of Medicine, Baltimore, MD, USA.

[3]Division of Dermatology, Department of Medicine, College of Human Medicine, Michigan State University, East Lansing, MI, USA.

[4]Department of Pharmacology and Toxicology, College of Human Medicine, Michigan State University, East Lansing, MI, USA.

[5]Institute for Quantitative Health Science & Engineering, Michigan State University, East Lansing, MI, USA.

[6]Department of Veterinary Pathobiology, School of Veterinary Medicine and Biomedical Sciences, Texas A&M University, College Station, TX, USA.

[7]Department of Entomology, Texas A&M University, College Station, TX, USA.

[8]Division of Environmental Health Sciences, School of Public Health, University of Minnesota, Minneapolis, MN, USA.

[9]Department of Biology, California State University San Marcos, San Marcos, CA, USA.

[10]Department of Entomology, University of Minnesota, Minneapolis, MN, USA.

[†]Present address: Rancho BioSciences, San Diego, CA, USA.

[‡]Present address: Immunology Program, Memorial Sloan Kettering Cancer Center, New York, NY, USA.

[§]Present address: Ribeirão Preto Medical School, University of São Paulo, Ribeirão Preto, SP, Brazil.

[#]Present address: Fiocruz-Bi-Institutional Translational Medicine Project, Ribeirão Preto, SP, Brazil.

*Corresponding author: jpedra@som.umaryland.edu

Abstract

Hematophagous ectoparasites, such as ticks, rely on impaired wound healing for skin attachment and blood feeding. Wound healing has been extensively studied through the lens of inflammatory disorders and cancer, but limited attention has been given to arthropod-borne diseases. Here, we used orthogonal approaches combining single-cell RNA sequencing (scRNAseq), flow cytometry, murine genetics, and intravital microscopy to demonstrate how tick extracellular vesicles (EVs) disrupt networks involved in tissue repair. Impairment of EVs through silencing of the SNARE protein *vamp33* negatively impacted ectoparasite feeding and survival in three medically relevant tick species, including *Ixodes scapularis*. Furthermore, *I. scapularis* EVs affected epidermal γδ T cell frequencies and co-receptor expression, which are essential for keratinocyte function. ScRNAseq analysis of the skin epidermis in wildtype animals exposed to *vamp33*-deficient ticks revealed a unique cluster of keratinocytes with an overrepresentation of pathways connected to wound healing. This biological circuit was further implicated in arthropod fitness when tick EVs inhibited epithelial proliferation through the disruption of phosphoinositide 3-kinase activity and keratinocyte growth factor levels. Collectively, we uncovered a tick-targeted impairment of tissue repair via the resident γδ T cell-keratinocyte axis, which contributes to ectoparasite feeding.

Introduction

Hematophagy evolved several times along independent pathways of arthropod evolution[1]. Nevertheless, blood-feeding of ticks stands out as distinctive among hematophagous arthropods due to their prolonged attachment to the host skin[2]. For instance, Ixodidae larvae and nymphs can feed for several days, while adults may require more than a week for hematophagy[3]. This presents unique challenges to the tick because it increases the risk of rejection from the host[3]. Thus, ticks have evolutionarily acquired salivary molecules that perturb inflammation, blood coagulation, and nociception to suppress host immunity and facilitate the attachment to the host skin[4-6].

Tick-borne microbial agents take advantage of the way tick saliva modifies host defenses, leading to the creation of a tolerant immune environment at the bite site that is conducive for pathogen transmission[7]. In North America, the most medically relevant genera for ticks are *Ixodes*, *Amblyomma*, and *Dermacentor*[8]. Notably, the blacklegged tick *Ixodes scapularis* transmits seven different human pathogens, including the Lyme disease spirochete *Borrelia burgdorferi* [9,10]. Additionally, the Lone star tick *Amblyomma americanum* transmits *Ehrlichia chaffeensis* and *E. ewingii* causing human ehrlichiosis, while the American dog tick *Dermacentor variabilis* and *D. andersoni* transmit *Rickettsia rickettsii* and *Francisella tularensis* resulting in Rocky Mountain spotted fever or tularemia, respectively[11]. Several studies of the vector-pathogen-host interface underscore the significance of tick saliva and skin immunity in the dissemination and persistence of vector-borne diseases[5,12].

As the largest organ in the body, the skin averts the loss of fluids and affords a protective barrier against microbial and environmental threats[13,14]. The skin is comprised of three primary layers: the outermost epidermis, the underlying dermis, and the hypodermis or subcutaneous fat[13,14]. The current paradigm is that tick salivary molecules are deposited within the dermis during feeding, where they actively regulate skin function[5,12]. Any impact on the epidermis, which interfaces with the external environment, has been mostly neglected. The significance of

the epidermis in countering tick infestation was documented in the late 1970s wherein Langerhans cells were shown to respond to salivary gland antigens[15]. Additionally, we recently reported that extracellular vesicles (EVs) within tick saliva affect the frequency of dendritic epidermal T cell (DETC) and alter the cytokine and chemokine milieu of the skin[16].

DETCs express the invariant T cell receptor Vγ5Vδ1[17] (also known as Vγ3Vδ1[18]) and are a subset of murine γδ T cells located in the epidermis. Importantly, DETCs have a critical role in wound healing and interact with keratinocytes, which comprise 95% of the epidermal layer[13,14]. Keratinocytes act as immune sentinels in the epidermal niche and express various immune genes that are activated by microbial perturbations and injury[19-22]. As a result, keratinocyte-derived cytokines, chemokines, and antimicrobial peptides facilitate interactions with immune cells, driving the process of wound healing[21,22]. In both homeostatic conditions and in the aftermath of an injury, DETCs secrete soluble factors, such as insulin-like growth factor I (IGF1) and keratinocyte growth factor (KGF)-1 and -2, that promote the survival and proliferation of epidermal cells, respectively[23-27]. Conversely, keratinocytes secrete interleukin (IL)-15 to maintain the tissue residency and self-renewal of DETCs[13,14].

The impact of DETCs in tissue repair during feeding of ectoparasites remains elusive. In this study, we combined single cell RNA sequencing (scRNAseq), murine genetics, intravital microscopy and flow cytometry to demonstrate how tick EVs disrupt networks involved in epidermal homeostasis. We identified a unique cluster of cells with an overrepresentation of pathways connected to wound healing during a bite of EV-deficient ticks. We further underpinned this biological network by demonstrating that tick EVs impacted epithelial cell proliferation through disruption of phosphoinositide 3-kinase (PI3K) activity and KGF levels. Collectively, we illustrate a tick-induced interference of tissue repair via the skin epidermis, contributing to the process of arthropod hematophagy.

Results

Tick EVs enable arthropod fitness. We previously observed that EVs from *I. scapularis* contribute to proper hematophagy[16]. We sought to corroborate these findings in several tick species of public health importance, such as *I. scapularis*, *A. americanum*, and *D. variabilis*, and measure how EVs affect arthropod fitness. Due to technical limitations of clustered regularly interspaced short palindromic repeats (CRISPR), modified tick strains are not yet available given their long-life cycle and the difficulties associated with manipulating their embryos[28]. Thus, we silenced the expression of the vesicle associated membrane protein 33 (*vamp33*) through RNA interference (RNAi) to study the effect of tick EVs[16].

We designated arthropods that had reduced *vamp33* expression due to the treatment with small interfering RNAs as si*V33*, EV-deficient ticks, and the scramble control treatment as sc*V33*, EV-sufficient ticks. Si*V33* and sc*V33* microinjected nymphs were placed on C57BL/6 mice and allowed to feed for 3 days (Fig. 1A). On day 3, *I. scapularis* were measured for efficiency of *vamp33* silencing, attachment, and collected for weight and post-feeding survival (Fig. 1B-E). We did not observe a difference in attachment between si*V33* and sc*V33* nymphs (Fig. 1C). However, diminished feeding was measured for EV-deficient ticks as demonstrated by a 53% reduction in tick weight (Fig. 1D). Interrupted feeding in *I. scapularis* led to reduced survival post-detachment (Fig. 1E). Similar results to *I. scapularis* were observed for both *A. americanum* and *D. variabilis* (Fig. 1F-M), affirming an EV-associated fitness in three medically relevant tick species. Collectively, these findings offer the prospect of a cross-species integrated management for tick infestation of mammals.

Tick EVs regulate DETCs in murine skin. Recent findings indicate that tick EVs exert an impact on mammalian DETCs[16]. We allowed *I. scapularis* nymphs to feed on mice for 3 days and then collected the skin biopsy for flow cytometry evaluation (Supplementary Figure 1). We observed a decrease of DETC frequency during sc*V33* tick feeding on mice compared to naïve

skin (Fig. 2A). Conversely, DETC frequency remained at homeostatic levels after impairment of tick EVs (si*V33*) and ectoparasite feeding on murine animals (Fig. 2A). Upon tissue damage, stressed keratinocytes upregulate ligands and antigens that stimulate DETCs in a non-major histocompatibility complex (MHC)-restricted manner[29]. Unlike conventional αβ T cells, DETCs lack accessory molecules such as CD4, CD8, or CD28, which are important for activation. On the other hand, they upregulate junctional adhesion molecule-like (JAML), the semaphorin CD100 (also known as SEMA4D) and the C-type lectin-like receptor NKG2D (also known as KLRK1) upon activation (Fig. 2B)[30-32]. We reasoned that tick EVs affected DETC co-receptor ligands and sought to examine the activation status during tick feeding. Co-receptor frequency was elevated among DETCs found at the location where EV-sufficient ticks fed on mice (Fig. 2C-F). Notably, JAML and NKG2D, two surface molecules important for DETC co-stimulation of keratinocytes[30,32], were not upregulated in the bite of EV-deficient ticks during murine feeding (Fig. 2C-D). Similar findings were also observed for the activation markers CD69 and CD25 (Fig. 2E-F).

Upon cutaneous damage, DETCs alter their morphology by retracting dendrites and assuming a rounded configuration to facilitate migration to the site of injury[27,33]. To capture morphological changes, we utilized a mouse model with distinct fluorescent markers that label three cell types within the skin epidermis[34]. These mice express GFP under the control of the *Cx3cr1* promoter and the histone H2B-Cerulean under the control of *Krt14* promoter to label DETCs and epithelial cells, respectively. Additionally, these mice contain *CD207-CreER;Rosa-stop-tdTomato* reporter that label Langerhans cells after tamoxifen injection. Intravital microscopy of EV injection into the ear of this mouse model revealed that tick EVs did not promote rounding of DETCs, as compared to the positive control nocodazole (Fig. 2G). Because this biological process is partially regulated through the CD100 signaling cascade[31], we evaluated the CD100 molecule by flow cytometry. Supporting epidermal intravital imaging findings, expression of CD100 was not altered during a tick bite regardless of the EV status (Fig.

2H). Collectively, these findings provided evidence that tick EVs functionally regulate DETCs in the murine skin.

ScRNA-seq characterization of epidermal cells during tick feeding. The elongated morphology of DETCs allows for constant interaction with neighboring cells, such as keratinocytes. Upon barrier breach, DETCs release cytokines to prevent infection, recruit immune cells, and produce growth factors crucial for keratinocyte proliferation and survival[33,35]. We reasoned that tick EVs might not solely impact DETCs, but also affect keratinocytes, thereby regulating epidermal homeostasis. To evaluate this hypothesis, we utilized scRNAseq to analyze the impact of tick EVs on the epidermal immune environment in both DETC-deficient (FVB-Tac) and DETC-sufficient (FVB-Jax) mice. FVB-Tac mice are depleted of functional DETCs due to a failure of thymic selection because of a natural mutation of the *skint1* gene[36-38]. Si*V33* ticks or sc*V33* were fed on FVB-Tac or FVB-Jax mice for 3 days. Skin punch biopsies were obtained from the bite site, and the epidermis was enzymatically separated from the dermis. Live cells were sorted by fluorescence activation and libraries were generated for Illumina sequencing (Fig. 3A).

Single cell data was aligned to the mouse genome and feature-barcode matrices were generated using the 10X Genomics Cell Ranger pipeline. Our analysis encompassed approximately 20,640 cells, with an average of 88,027 reads. Our initial investigation resulted in 23 clusters (Supplementary Dataset 1). Next, we applied a fixed threshold to retain cells with more than 2500 UMIs (Supplementary Figure 2A-B) and applied the DoubletFinder R package to predict doublets (Supplementary Figure 2C-D). We identified 10 distinct groups of cells through an analysis of marker genes within each cluster relative to the entire dataset (Supplementary Dataset 2). Keratinocytes, T cells, fibroblasts and endothelial cells were observed in our scRNAseq results (Supplementary Figure 2D). The presence of dermal populations in our study was likely due an incomplete epidermal-dermal border separation

during the enzymatic dissociation of skin biopsies. Thus, we subjected keratinocytes, T cells, and antigen-presenting cells (APCs) to a second round of clusterization (Supplementary Dataset 3). This dataset revealed a total of 8 clusters visualized in t-distributed stochastic neighbor embedding (t-SNE) (Fig. 3B) for a total of 5,172 total cells with a median UMI count of 13,910 per cell.

Throughout the process of differentiation, keratinocytes express different types of keratins, including keratins (Krt) 1, 5, 10, and 14[39]. Elevated levels of *Krt5* and *Krt14* expression enabled the recognition of undifferentiated cells residing within the basal layer of the epidermis (Fig. 3C, Supplementary Dataset 4). *Krt1*, *Krt10*, and *involucrin* were used to discern early and late stage differentiation of keratinocytes (Fig. 3C, Supplementary Figure 3, Supplementary Dataset 4). APCs and T cells were identified by the T cell receptor alpha constant (*Trac*), the T cell receptor delta constant (*Trdc*), and the histocompatibility class II antigen (*H2-Aa*) (Supplementary Dataset 3, Supplementary Table 2). The mouse epidermis harbors hair follicles with distinct physiological functions[39,40]. Our dataset only accounted for compartments in anatomical proximity to the epidermis (Supplementary Figure 4, Supplementary Table 2).

We then determined the percent distribution of interfollicular epidermal cells per treatment. In the skin biopsy where ticks fed on immune intact mice (FVB-Jax sc*V33* and FVB-Jax si*V33*), we observed a decrease in keratinocytes and an overrepresentation of T cells and APCs compared to the naïve skin (Fig. 3D, Supplementary Dataset 5). A similar effect was not observed when ticks fed on the skin of DETC-deficient mice (Fig. 3E, Supplementary Dataset 5), presumably due to the diminished wound healing capacity in FVB-Tac animals[41]. We confirmed the depletion of DETCs in the epidermis of FVB-Tac mice. Gene expression of *Trdv4* in the T cell cluster, which encodes for the receptor Vδ1 in DETCs, was reduced in FVB-Tac compared to the FVB-Jax mouse strain (Fig. 3F).

After partitioning epidermal clusters by experimental conditions, we observed an unidentified keratinocyte population found solely when EV-deficient ticks fed on FVB-Jax mice

(Supplementary Figure 5, Supplementary Dataset 3). The presence of this distinct cluster raised the hypothesis that EVs might exert an influence on keratinocytes within the context of DETCs, given its absence in FVB-Tac mice (Supplementary Figure 5D-F). We therefore moved forward with the analysis of keratinocytes and subjected these cells to a subsequent round of clustering. This examination revealed undifferentiated, early, and late stage differentiating keratinocytes in addition to the unidentified epidermal subpopulation (Fig. 3G, Supplementary Dataset 6).

Next, we relied on pseudotime to order keratinocytes along an inferred developmental trajectory based on their expression profile (Fig. 3H)[42]. Gene expression signatures mirrored the sequence of differentiation, starting with markers associated with undifferentiated basal states to terminally differentiated keratinocytes (Supplementary Figure 6)[43]. Importantly, the unidentified keratinocyte population was present along the pseudotime axis of the condition where EV-deficient ticks fed on FVB-Jax mice (FVB-Jax si*V33*), setting it apart from the other treatments (Fig. 3H). Taken together, we uncovered a keratinocyte population only present when EV-deficient ticks fed on mice carrying γδ T cells located in the epidermis.

Tick EVs impact wound healing through the DETC-keratinocyte axis. To investigate the properties of the unidentified population described above, we then separated keratinocytes according to their respective experimental conditions (Fig. 4A-F). This analysis revealed a population of cells present in the FVB-Jax si*V33* treatment (Fig. 4C) but absent in the FVB-Tac group (Fig. 4F). Pathway enrichment analysis of these unique keratinocytes revealed an overrepresentation of genes associated with growth factors, collagen, fibronectin, heparin binding, and phosphoinositide 3-kinase (PI3K) activity (Fig. 4G, Supplementary Dataset 7). These molecules have been implicated in keratinocyte proliferation, contributing to re-epithelization and tissue repair of the skin[44-46]. Thus, we hypothesized that tick EVs were impairing wound healing through the crosstalk between DETCs and keratinocytes. To test our hypothesis, we assessed keratinocytes originated from the FVB-Jax mice upon feeding of EV-

sufficient and compared to EV-deficient ticks. Wound healing networks were overrepresented through ingenuity pathway analysis (IPA) (Fig. 4H, Supplementary Dataset 8). Our dataset also unveiled a decrease in transcript levels for *Fos* and *Jun* and an increase of expression for *Col1a1* and *Col1a2* (Fig. 4I, Supplementary Dataset 9). *Fos* and *Jun* are subunits of AP-1, which is important for epithelial proliferation and differentiation[47,48]. Conversely, collagen binding reinforces barrier integrity and improves the stratification of epidermal layers[46]. Finally, this unique keratinocyte cluster showed elevated expression of *Col1a1*, *Col1a2*, and *Col3a1* compared to the remaining epidermal cells (Fig. 4J-K). Collectively, tick EVs impaired wound healing by affecting a biological circuit in keratinocytes.

Tick EVs interfere with keratinocyte proliferation. To understand how tick EVs affected this wound healing circuit in keratinocytes, we evaluated molecular networks altered in the epidermis of FVB-Jax and compared to the FVB-Tac mice. We also performed a similar analysis in naïve animals to exclude confounding effects originated from genetic differences occurring between these two strains. Four pathways were identified: eukaryotic Initiation Factor 2 (EIF2), natural killer (NK) cell, sirtuin signaling, and the unfolded protein response (UPR) (Fig. 5A, Supplementary Dataset 8). NK cell, sirtuin signaling, and the UPR pathways were likely due to the *skint1* deficiency in FVB-Tac mice. However, the EIF2 cascade was dependent on tick EVs because the computational prediction occurred regardless of the mouse genetic background (yellow highlight, Fig. 5A).

A granular view of the EIF2 signaling pathway displayed PI3K as part of the biological circuit targeted by tick EVs (Fig. 5B, Supplementary Dataset 10). The PI3K/Akt pathway is important for skin development and wound healing, two processes dependent on keratinocyte proliferation and differentiation[49]. Upon injury, cells adjacent to the wound are quiescent whereas cells located at a distance start to proliferate. Given that the PI3K/Akt/mTOR pathway has been observed in the proliferative zone and correlate with accelerated wound closure[50], we

reasoned that tick EVs interfered with keratinocyte proliferation. To evaluate this hypothesis, we used the protein Ki-67 and flow cytometry as a readout for proliferative keratinocytes (Supplementary Figure 7). We observed a significant reduction in keratinocyte proliferation when EV-sufficient ticks fed on wildtype mice (white bars – *scV33*, Fig. 5C). However, the effect of keratinocyte proliferation was not observed in the absence of tick EVs (white bars – *siV33*, Fig. 5C). As noted above, the impact of tick feeding on keratinocyte proliferation was fully dependent on DETCs. In the absence of DETCs, the observed phenotype for keratinocyte proliferation in EV-sufficient ticks did not occur (gray bars, Fig. 5C). Collectively, our reductionist approach orthogonally validated our scRNAseq results.

The genetic constitution of a mouse may lead to substantial alterations in phenotypic traits[51,52]. We therefore investigated the ability of *I. scapularis* to interfere with keratinocyte homeostasis in C57BL/6 mice. We ascertained the keratinocyte PI3K status by flow cytometry due to its ability to assess protein expression on limited cell counts. Variation in the total PI3K comparing keratinocyte populations among treatments was not observed (Fig. 5D). However, a decrease in phospho-PI3K-positive keratinocytes was recorded when ticks deficient in EVs fed on C57BL/6 mice (Fig. 5E). Additionally, the bite of *I. scapularis* ticks reduced levels of the growth factor KGF in keratinocytes compared to the EV-deficient treatment (Fig. 5F). A significant decline in the frequency of $EpCAM^{+}$ $Ki67^{+}$ keratinocytes was evident when EV-sufficient ticks fed on C57BL/6 mice (Fig. 5G). Remarkably, the ability of ticks to impair keratinocyte proliferation was observed in a quantitative-dependent manner. As the number of ticks feeding on C57BL/6 mice increased, the capacity of keratinocytes to proliferate decreased (Fig. 5H). This observation was not revealed in mice infested with ticks deficient for EVs (Fig. 5I). In summary, we uncovered that tick EVs impacted keratinocyte proliferation by suppressing KGF and PI3K activity, thereby, maintaining successful hematophagy.

Discussion

In this study, we sought to understand how tick EVs impact the epidermal circuitry during hematophagy. Although the role of EVs has been extensively studied in mammalian systems, their function in ectoparasitology remains elusive. Here, we established the importance of EVs for arthropod fitness in three medically relevant tick species: *I. scapularis*, *A. americanum*, and *D. variabilis*. We demonstrated that tick EVs led to a decrease in DETCs at the bite site; yet the DETCs that were present in the skin epidermis during hematophagy displayed upregulated co-stimulatory molecules. Collectively, these data suggested that tick EVs may target activated DETCs to disrupt epidermal function and enable successful blood feeding. Activation of DETCs occurs in response to keratinocyte-specific molecules during tissue damage. For DETCs to produce growth factors and participate in wound repair, the presence of the TCR is essential[53]. Although TCR genes are assembled by somatic recombination in DETCs, these T cells function in an innate-like manner by employing rapid effector responses[54]. Humans lack a direct equivalent of a DETC compartment, but they harbor tissue associated Vδ1$^+$ γδ T cells in the skin[54,55]. For example, clinical studies in the skin examined after tick infestation display impaired T cell responses and lower levels of intracellular IFNy[56]. Given the relationship between a defined TCR and its function in anatomical settings, we suggest that knowledge derived from murine animals may be applicable in clinical trials.

Reduction of DETCs at the bite site of ticks could be a result of cell death or cellular migration. Intraepidermal migration of DETCs is facilitated by the conversion of a dendrite to a rounded morphology[27], which is partially regulated by CD100 signaling[31]. To capture morphological changes, we employed intravital microscopy of EV injection into the ear of a triple-reporter mouse model[34]. Our results suggested that DETCs may not migrate during tick feeding due to the lack of cell rounding and CD100 upregulation. Wound healing consists of four main phases that occur in a temporal sequence: 1) hemostasis, 2) inflammation, 3) proliferation, and 4) remodeling[57]. DETCs are mainly involved in the inflammation and proliferation phases of

wound healing because the timely resolution of cutaneous wounds is delayed in their absence[27,33,35]. Using a scRNAseq approach, we confirmed that naïve FVB-Tac mice had a decreased frequency in the keratinocyte cluster, suggesting increased apoptosis in epidermal cells due to the lack of DETCs[23,41]. Further analysis revealed a unique keratinocyte population when EV-deficient ticks fed on DETC-sufficient animals. Enrichment analysis of this cluster showed overrepresentation of pathways associated with cell proliferation. Moreover, specific biological signatures were associated with down regulation of AP-1 and upregulation of collagen and PI3K transcripts in EV-deficient ticks fed on FVB-Jax mice. These molecular circuits have been linked to epithelial proliferation and maintenance of barrier integrity[46-48,58].

Consistent with our systems level approach, EV-sufficient ticks fed on FVB-Jax mice led to a decrease in keratinocyte proliferation. Importantly, this wound healing observation was fully dependent on the role of DETCs. Notably, wound healing is marked by keratinocyte proliferation and migration to restore barrier function of the epidermis[57]. For instance, proliferation was deemed as a necessary step for proper wound closure at the leading edge in the murine tail[59]. Conversely, proliferation was judged dispensable for wound closure in the murine ear[60]. Our work was done using the natural site of tick infestation in mammals, the skin of the dorsal neck. Whether proliferation is necessary for migration during a tick bite remains to be determined.

Variation in the genetic background of a mouse strain can result in significant changes in molecular functions[51,52]. Hence, we utilized FVB-Jax and FBV-Tac strains to acquire insights into EV regulation within the context of DETCs. Subsequently, we transitioned these findings to the C57BL/6 strain to validate our results. Multiple cell types, growth factors, and signaling circuitries have been implicated in wound healing of the skin[57]. We postulated that tick EVs interfered with these components, including PI3K and the growth factor KGF. We observed decreased levels of phosphorylated PI3K during EV-sufficient tick feeding on C57BL/6 mice, mirroring the findings from the scRNAseq studies on FVB mice. KGF serves as a strong mitogenic factor for both mouse and human keratinocytes, and its overexpression can lead to a

hyperproliferative state associated with skin disorders[61]. We observed that tick feeding on mice led to decreased KGF levels compared to the EV-deficient treatment. The observed reduction in DETC levels during tick feeding may obstruct the local generation of KGF in the epidermis.

Finally, extracts from tick salivary glands have shown their capability to bind growth factors and impede cellular growth *in vitro*[62]. Accordingly, we demonstrated *in vivo* that tick EVs led to a significant reduction in the frequency of $Ki67^{+}$ keratinocytes. Strikingly, the ability of ticks to impair epithelial cell proliferation was observed in a quantitative-dependent manner. The more ticks fed simultaneously at a given site, the less keratinocytes were able to proliferate. Collectively, this study unveiled the immunomodulatory potential of tick EVs within the skin epidermal environment during hematophagy. These findings are a significant departure from the viewpoint established by the scientific community where arthropod saliva affects the skin dermis.

Materials and Methods

Reagents and resources

All primers, reagents, resources, and software used in this study, together with their manufacturer's information and catalog numbers are listed in Supplementary Tables 1 and 3.

Ticks

I. scapularis nymphs were obtained from two independent sources: (1) Dr. Ulrike Munderloh and Dr. Jonathan Oliver at the University of Minnesota; and the (2) tick rearing facility at Oklahoma State University. *A. americanum* and *D. variabilis* nymphs were obtained from the tick rearing facility at Oklahoma State University. Partially engorged *I. scapularis* adult ticks were obtained from Dr. Albert Mulenga and Dr. Adela Oliva Chavez at Texas A&M University. Upon arrival, ticks were maintained in a Percival I-30BLL incubator at 23°C with 85% relative humidity and a 12/10-hours light/dark photoperiod regimen.

Mice

Experiments were performed on C57BL/6, FVB/N Jax, and FVB/N Tac mice. Breeding pairs were purchased from the Jackson Laboratory except FVB/N Tac mice, which were purchased from Taconic Biosciences. All mouse strains were bred at the University of Maryland School of Medicine, unless otherwise indicated. Male mice (7–9 weeks) were used for all experiments. All mouse experiments were approved by the Institutional Biosafety (IBC-00002247) and Animal Care and Use (IACUC, #0119012) committees at the University of Maryland School of Medicine and complied with the National Institutes of Health (NIH) guidelines (Office of Laboratory Animal Welfare [OLAW] assurance number A3200-01). *huLangerin-CreER;Rosa-stop-tdTomato;CX3CR1-GFP*$^{+/-}$*;K14-H2B-Cerulean* mice used for intravital microscopy imaging were housed at Michigan State University as described elsewhere[34].

377

378 **RNA interference**

379 siRNAs and scRNAs for *vamp33* were designed as previously described[16]. Both siRNAs
380 and scRNAs were synthesized according to the Silencer® SiRNA construction kit (Thermo
381 Fisher Scientific). Primers are described in Supplementary Table 1. Unfed nymphs were
382 microinjected with 60-80 ng of siRNA or scRNA using a Nanoject III (Drummond Scientific
383 Company). Ticks recovered overnight at 23°C with saturated humidity.

384

385 **EV-depleted media**

386 L15C300 medium was supplemented with 5% FBS (Millipore-Sigma), 5% tryptose
387 phosphate broth (TPB) (BD), 0.1% lipoprotein concentrate (LPC) (MP Biomedicals), 0.25%
388 sodium bicarbonate (Millipore-Sigma), and 25 mM HEPES (Millipore-Sigma). Media was cleared
389 from EVs by ultracentrifugation at 100,000×g for 18 h at 4 °C in a LE-80 ultracentrifuge
390 (Beckman Coulter) with a 60Ti rotor. EV-free media was then passed through a 0.22-µm
391 Millipore Express® PLUS (Millipore-Sigma). The absence of EVs was confirmed by determining
392 the particle size distribution with the NanoSight NS300 (Malvern Panalytical) for nanoparticle
393 tracking analysis (NTA).

394

395 **Tick salivary gland culture**

396 Salivary gland EVs were purified from *ex vivo* cultures that originated from partially
397 engorged adult female ticks. Adult *I. scapularis* females were fed on New Zealand white rabbits
398 for 5–6 days at either Dr. Albert Mulenga or Dr. Adela Oliva Chavez laboratories at Texas A&M
399 University, as previously described[63]. Then, ticks were shipped to the University of Maryland
400 School of Medicine. Partially-fed adult female ticks (90-120) were dissected 1–2 days post-
401 removal. Briefly, midguts, Malpighian tubes, and other organs were removed. PBS was added to
402 samples to avoid desiccation. Salivary glands were dissected and cultured in 24-well cell culture

plates (Corning). 10 salivary glands from adult ticks were placed in each well, containing 500 µl of L15C300 EV-free medium supplemented with 1x penicillin/streptomycin (Corning) and 1x Amphotericin B (Gibco). Salivary glands were incubated for 24 h at 34 °C to allow EV secretion.

EV purification

Tick EVs were isolated as previously described[16]. Medium collected from salivary gland cultures were cleared of any live cells by centrifugation at 300 × g for 10 minutes at 4 °C. Dead cells were removed by a second centrifugation at 2,000 × g for 10 minutes at 4 °C. The supernatant was collected, and apoptotic bodies were removed by a third centrifugation at 10,000 × g for 30 minutes at 10°C. The supernatant was filtered through a 0.22-µm Millipore syringe filter (Millipore-Sigma) to reduce the number of EVs >200 nm in size. EVs were pelleted by ultracentrifugation (100,000 × g) for 18 hours at 4 °C. Supernatant was discarded and EVs were resuspended in PBS. EV concentration and sizes were determined using the NanoSight 300 machine (Malvern Panalytical) with the software versions 2.0 or 3.0. The mean of the size generated in the reports was used to calculate the average size of the EVs in each sample. The concentration of proteins in tick EVs was determined using the BCA assay (Thermo Scientific), following the manufacturer's procedure.

Mouse capsule placement

Capsules made from the upper portion of a snap or screw top tube were adhered to the dorsal neck of each mouse to contain the ticks in one area. This technique is referred to as the capsule-feeding method and was adapted from a previous study[64]. Briefly, capsule adhesive solution was made from 3 parts gum rosin (Sigma-Aldrich) and 1 part beeswax (FisherScience). Mice were anesthetized using isoflurane and shaved between the shoulder blades to the top of the cranium. Capsules were applied with the warmed adhesive and allowed to dry up for 24

hours prior to tick placement. Capsules were sealed with either a glued piece of mesh or a screw top.

Tick feeding experiments

Microinjected ticks were placed on mice using either the free-feeding or capsule-feeding method and allowed to feed for 3 days. On day 3, ticks were collected, weighed, and either placed in a humidified chamber for survival analysis or frozen at −80°C for RNA purification. To purify the mRNA, ticks were flash-frozen in liquid nitrogen and crushed with small plastic pestles. TRIzol® reagent (200 µl) was added to the crushed tick and RNA was purified using the PureLink™ RNA mini kit. cDNA was synthesized from 50 to 200 ηg (5–10 µl) of RNA using the Verso cDNA synthesis kit (Thermo scientific).

Quantitative reverse transcription polymerase chain reaction (qRT-PCR)

qRT-PCR was performed to measure gene expression. qRT-PCR was performed with the CFX96 Touch Real-Time PCR Detection 233 System (Biorad). No template controls were included to verify the absence of primer-dimers formation and/or contamination. Reactions on each sample and controls were run in duplicate. Gene expression was determined by relative quantification normalized to the tick *actin*, using the primers listed in Supplementary Table 1.

Flow cytometry of skin cell populations

I. scapularis nymphs fed on C57BL/6, FVB/N Jax, or FVB/N Tac male mice. On the third day of feeding, mice were euthanized with CO_2. A 10- or 5-mm skin punch biopsy was taken while ticks were still attached. Skin samples from un-infested control mice were collected from matching locations. Single cell suspensions were prepared from each skin sample. Briefly, skin samples were cut into small pieces with sterile surgical scissors and placed into round-bottom tubes containing digestion buffer consisting of 90% RPMI-1640 (Quality Biological), 10%

Liberase™ TL Research Grade (Roche), and 0.1% DNAse I (Millipore-Sigma). Digestions were carried out for 1 hour and 15 minutes at 37°C with constant shaking. Single cell suspensions were obtained by passing the digested tissues through a 40-µm cell strainer (Corning), homogenizing the tissue with a plunger and flushing cells with wash buffer consisting of PBS and 2 mM EDTA. Cells were centrifuged at 300 x g for 5 minutes at 4 °C, resuspended in 1 ml FACS buffer (PBS containing 1% BSA, 2 mM EDTA, and 0.05% NaN3) or FACS intracellular buffer (PBS containing 1% BSA and 0.05% NaN3). Cell suspensions were placed into a 96-well U-bottom plate and stained with respective antibody panels.

Live and dead cells were discriminated using Zombie Violet Fixable Live Dead stain (BioLegend). Cells were washed with FACS buffer. Cells were then blocked with anti-FcR (CD16-CD32) (BioLegend 156603), and subsequently stained with the respective antibody panel for 15 minutes at 4°C and washed with FACS buffer. Whenever appropriate, anti-rat IgM was added to the cells, incubated for 15 minutes at 4°C, and washed twice with the FACS buffer. Finally, cells were resuspended in 4% paraformaldehyde. For intracellular staining, cells were further processed following the instructions for the BioLegend's FOXP3 Fix/Perm Buffer Set kit. Cells were measured with a LSRII flow cytometer (BD) at the Flow & Mass Cytometry Facility at the University of Maryland School of Medicine. Analysis was performed using the FlowJo software.

DETC populations in the murine skin were labeled with APC anti-CD45 (BioLegend 103111) or PE/Cyanine7 anti-CD45 (BioLegend 103114), FITC anti-CD3 (BioLegend 100203), BV60 anti-Vγ5 (BD 743241), APC anti-Thy1.2 (BioLegend 105312), and/or monoclonal antibody 17D1 (kindly provided by Dr. Adrian Hayday, King's College London, and Dr. Robert Tigelaar, Yale University), and PE mouse anti-rat IgM (BD 553888). DETC costimulatory markers were measured with PE anti-JAML (BioLegend 128503), BV711 anti-CD100 (BD 745492), PE/Cyanine5 anti-CD44 (BioLegend 103010), APC/Cyanine7 anti-CD25 (BioLegend 102026), PerCP/Cyanine5.5 anti-CD69 (BioLegend 104522), and APC anti-CD314 (BioLegend 130212).

Keratinocyte populations in the murine skin were labeled with BV711 anti-CD324 (BioLegend 118233), PE anti-CD200 (BioLegend 123807), PE/Cyanine5 anti-CD34 (BioLegend 119312), BV605 Sca1 (BioLegend 108133), and/or PE anti-CD49f (BioLegend 313612). Keratinocyte proliferation was labeled with the Alexa Fluor 700 anti-Ki-67 (BioLegend 652420).

Intravital microscopy

Epidermal intravital imaging studies were done in collaboration with Dr. Sangbum Park at Michigan State University. All *in vivo* imaging and analysis were performed, as described previously[34]. Simultaneous visualization of Langerhans cells, DETCs and epithelial cells was achieved by utilizing the *huLangerin-CreER;Rosa-stop-tdTomato;CX3CR1-GFP*$^{+/-}$*;K14-H2B-Cerulean* mice.

Epidermal single-cell isolation, scRNA-seq library preparation and sequencing

I. scapularis nymphs were microinjected with *vamp33* si or *vamp33* sc and fed on FVB/N Jax or FVB/N Tac mice. On the third day of feeding, mice were euthanized with CO_2. Partially fed ticks were removed and the sites where ticks bit were shaved followed by an application of a light layer of Nair depilatory lotion. A total of three 5-mm skin punch biopsies were obtained from the dorsal neck for each mouse. 5-mm skin punch biopsies were obtained from the same physiological site of naïve mice. Skin samples were incubated in dispase solution (4 U/mL dispase, 5mM MgCl2, and 0.4mM CaCl2 in PBS) for 2.5 hours at 37°C with constant shaking/stirring. Epidermal sheets were separated from the dermal layer using forceps. Epidermal sheets were then incubated in a digestion solution (2.5mg/mL collagenase D and 0.2mg/mL DNase in RPMI Medium) for 1 hour at 37°C with constant shaking/stirring.

Cells were resuspended using a wide-bore pipette tip and three samples per treatment per mouse were combined. Samples were passed through a 40 µM cell strainer and washed with RPMI +10% FBS. Cells were counted using the Countess II FL Automated Cell Counter,

stained with 5 µl of 7-AAD per million cells, and incubated in the dark for 10 minutes at 4°C. Samples were then sorted at the CIBR Flow Cytometry Core Facility at the University of Maryland School of Medicine. Cells were sorted into a PBS in the absence of calcium and magnesium + 10% FBS collection buffer. They were then transported on ice to the Institute of Genome Sciences at the University of Maryland School of Medicine for library preparation and sequencing. Single cell libraries were generated with the 3' NextGEM v3.1 kit targeting 3800-5000 cells. Libraries were sequenced with a NovaSeq 6000, S2 flowcell targeting 375M read pairs per sample.

Bioinformatics

All scRNA-seq reads were processed and mapped to the mouse mm10 reference genome using 10X Genomics' Cell Ranger software. Approximately 20,640 total cells were profiled with 88,027 mean reads per cell across all conditions. A count matrix (gene-by-cell) generated by cell ranger count for each library was then aggregated into a single count matrix. Expression matrices were generated using the Bioconductor packages scater (v1.22.0)[65] and scran (v1.22.1)[66]. Cells with less than 2,500 or greater than 60,000 UMIs were removed after calculating cell metrics using scater (v1.22.0). DoubletFinder (v2.0.1)[67] was applied removing 1,364 cells, which yielded a total of 10,715 cells. The remaining transcriptomes were normalized by first calculating size factors via the scran functions quickCluster and computeSumFactors. Then, we computed normalized counts for each cell with logNormCounts function in scran (v1.22.1).

For downstream analysis, highly variable genes were selected using getTopHVGs before performing the Principal Component Analysis (PCA) and the tSNE projection. Clustering was conducted using kmeans function based on the calculated tSNE. Differential gene expression between clusters was calculated using find Markers function. Only identified epidermal cells of interest (Keratinocytes, T cells, and APCs) were further analyzed, resulting in a total of 5,172

cells with a median UMI count of 13,910 per cell. For pseudotime analysis, the Bioconductor matrix was imported into slingshot (v2.2.1)[68]. To compare the T cell receptor delta variable 4 (*Trdv4*) expression, normalized counts were used for visualization by the violin plot. The permutation test was applied to calculate the significance of the difference in the mean expression between two groups. A list of differentially expressed keratinocyte genes between treatments was generated by MAST (v1.24.0)[69] with significance testing under the Hurdle model for downstream analysis by the IPA.

Gene set enrichment analysis

Gene set enrichment analysis was performed using DAVID, version 2021. Default DAVID parameters were employed and included the following categories for the enrichment analysis: GOTERM_BP_DIRECT, GOTERM_CC_DIRECT and GOTERM_MF_DIRECT (from Gene_Ontology), KEGG_PATHWAY (from Pathways) and INTERPRO (from Protein_Domains). *p* value and FDR< 0.05 were set as a threshold.

Ingenuity pathway analysis

Differentially expressed keratinocyte genes from the following samples were analyzed in the IPA as independent datasets: 1) FVB-Tac Naïve versus FVB-Jax Naïve 2) FVB-Jax si*V33* versus FVB-Jax sc*V33* and 3) FVB-Tac si*V33* versus FVB-Tac sc*V33*. Genes were considered differentially expressed if the *p* value and FDR were < 0.05. Dataset input criteria for the IPA included expression, *p* value, log ratio, FDR, and Ensemble ID codes. All datasets were examined for canonical pathway and upstream regulator analysis. FVB-Tac Naïve versus FVB-Jax Naïve dataset had 591 IDs, including 589 mapped and 2 unmapped IDs. FVB-Jax si*V33* versus FVB-Jax sc*V33* dataset had 1207 IDs, including 1204 mapped and 3 unmapped IDs. FVB-Tac si*V33* versus FVB-Tac sc*V33* had 732 IDs, including 728 mapped and 4 unmapped IDs. The IPA proprietary algorithm segments the network map between molecules into multiple

558 networks and assigns scores for each network as described previously[70]. For the canonical
559 pathway analysis, −log (P-value) >2 was taken as threshold and for the upstream regulator
560 analysis, the *p* value of overlap <0.05 was set as the threshold. A positive *Z*-score was defined
561 as the predicted activation, and a negative *Z*-score was defined as the predicted inhibition.
562
563 **Statistical analysis**
564 Statistical significance was assessed as follows: percent tick attachment was calculated
565 by the Fisher's exact test, tick weight by the *t* test or the Mann Whitney test, and survival curve
566 by the Log-rank (Mantel-Cox) test. One-way ANOVA followed by Tukey's *post hoc* test for
567 multiple comparisons was also used. Kruskal-Wallis ANOVA was implemented if the dataset
568 failed normality of residuals or displayed heterogeneity of variance. We used GraphPad
569 PRISM® (version 9.1.0) for all statistical analyses. Outliers were detected by a Graphpad
570 Quickcals program (https://www.graphpad.com/quickcalcs/Grubbs1.cfm).

Acknowledgements

We acknowledge members of the Pedra laboratory for providing insightful discussions. We thank the rearing facility at Oklahoma State University for providing *I. scapularis, A. americanum,* and *D. variabilis* ticks; Xiaoxuan Fan, Bryan Hahn, Regina Harley, and Sean McGill (University of Maryland School of Medicine) for flow cytometry and sorting assistance; Adrian Hayday (King's College London) and Robert Tigelaar (Yale University) for the monoclonal antibody 17D1; the Maryland Genomics Core at the Institute for Genome Sciences, University of Maryland School of Medicine for the services provided in next generation sequencing; the University of Maryland Greenebaum Comprehensive Cancer Center Flow Cytometry Shared Service core facility and the Flow & Mass Cytometry Facility at the University of Maryland School of Medicine for flow cytometry services; Cristiana Cairo, Nevil Singh, Nicholas Carbonetti (University of Maryland School of Medicine) and Jere McBride (University of Texas Medical Branch) for insightful advice. This work was supported by grants from the NIH to F31AI152215 (AJO), F31AI167471 (LRB), R01AI134696 (JHFP), R01AI116523 (JHFP), P01AI138949 (JHFP), T32AI162579 (HJL-Y), R01AR083086 (SP), the United States Department of Agriculture, National Institute of Food and Agriculture (USDA-NIFA) Hatch-Multistate Project to TEX0-1-7714 (AOC), and the Knipling-Bushland-Swahrf fellowship from the Department of Entomology at Texas A&M University (BL-G). The content is solely the responsibility of the authors and does not represent the official views of the NIH, the Department of Health and Human Services, the USDA-NIFA or the United States government.

Data and Code Availability

All scRNA sequences are deposited into the NCBI Sequence Read Archive under the BioProject accession PRJNA905677. R codes for scRNA sequencing datasets were adapted from https://bioconductor.org/books/3.16/OSCA/ and specified R package vignettes. Tokens can be made available upon request.

Resource Availability

Further information and request for resources and reagents should be directed to and will be honored by the corresponding author: Joao HF Pedra (jpedra@som.umaryland.edu)

Author contributions

LM and JHFP designed the study. LM and LMV performed the experiments. HNB, HJL-Y and AR performed computational analysis. AJO, LRB, CRF, ADS-S, DMR, MTM, SS, NS, and FECP aided with experimentation. EBC, T-TN, BL-G, ASOC, AM, UGM and JDO provided ticks. LM and JHFP wrote the manuscript. LRB created illustrations. VMB, JMJ, SP, and DS supervised experiments and/or provided resources and guidance. JHFP supervised the study. All authors analyzed the data, provided intellectual input into the study, and contributed to editing of the manuscript.

Figure Legends

Figure 1: Tick EVs affect hematophagy and survival. (A) Graphical illustration of experimental design. **(B-M)** *Vamp33* siRNA (si*V33*) (red) or *vamp33* scramble control (sc*V33*) (blue) microinjected nymphs were placed on C57BL/6 mice and allowed to feed for 3 days. On day 3, ticks were harvested and assessed for fitness measurements. Efficiency of *Vamp33* silencing and tick attachment, weight, and survival curves for **(B-E)** *I. scapularis*, **(F-I)** *A. americanum* and **(J-M)** *D. variabilis*. Graphs represent at least three independent experiments combined. Statistical significance shown as *p<0.05, ns = not significant. RNAi silencing was calculated by using the *t* test **(B, F, J)**. Attachment was calculated by the Fisher's exact test **(C, G, K)**, weight by the Mann Whitney test **(D, H, L)** and survival curve by Log-rank (Mantel-Cox) test **(E, I, M)**.

Figure 2: Tick EVs regulate DETCs during hematophagy. *I. scapularis* sc*V33* (blue) or si*V33* (red) ticks were placed on C57BL/6 mice and allowed to feed for 3 days. On day 3, biopsies were taken from the skin at the bite site and compared to the naïve treatment (gray). **(A)** DETC (Vγ5), **(C)** JAML, **(D)** NKG2D, **(E)** CD69, **(F)** CD25 and **(H)** CD100 cells were assessed by flow cytometry. Graphs represent 1 of 3 independent experiments. **(B)** Schematic representation of the DETC-keratinocyte crosstalk at the skin epidermis. **(G)** Epidermis containing Langerhans cells (red), DETCs (green), and keratinocytes (white) imaged on day 3 after injection with phosphate buffered saline (PBS - mock) or EV ($4x10^7$ particles) into the mouse ear. Nocodazole (100 µg/ml) was applied topically on the mouse ear to induce DETC rounding as a positive control. Langerhans cells, DETCs and epithelial cells were simultaneously visualized in the *huLangerin-CreER; Rosa-stop-tdTomato; CX3CR1-GFP$^{+/-}$; K14-H2B-Cerulean* mouse strain. Cre expression was induced with an intraperitoneal injection of tamoxifen (2 mg). Statistical significance shown as *p<0.05, ns = not significant. Data are presented as a mean with

standard deviation. Significance was measured by One-way ANOVA followed by Tukey's *post hoc* test.

Figure 3: Epidermally-enriched scRNA seq of the tick bite site. (A) Overview of the experimental design. Sc*V33* and si*V33 I. scapularis* nymphs were placed on FVB-Jackson (FVB-Jax) or FVB-Taconic (FVB-Tac) mice and fed for 3 days. Skin biopsies at the bite site were digested with dispase and collagenase for epidermal cell isolation. Cells were sorted and prepared for scRNAseq. **(B)** Composite tSNE plot of keratinocyte, T cell and antigen presenting cell clusters in FVB-Jax and FVB-Tac mice in the presence or absence of *I. scapularis* nymphs microinjected with sc*V33* or si*V33*. tSNE plot represents 5,172 total cells following filtration as described in the materials and methods. **(C)** Heatmap depicting expression of the top 5 marker genes present in clusters from the epidermally enriched tSNE plot clusters (as shown in **B**). **(D** and **E)** Cluster frequency of keratinocytes, antigen presenting and T cells in **(D)** FVB-Jax and **(E)** FVB-Tac mice. **(F)** Violin plot displaying the expression of the TCR-Vδ1 gene, *Trdv4*, in the epidermal T cell cluster of naive FVB-Jax or FVB-Tac mice. Significance shown as **p*<0.05 based on a permutation test using R statistical packages. **(G)** Composite tSNE plot of keratinocyte clusters in FVB-Jax and FVB-Tac mice in the presence or absence of *I. scapularis* nymphs microinjected with sc*V33* or si*V33*. **(H)** Cells colored by clusters originated from the keratinocyte tSNE plot (as shown in **F**) ordered across pseudotime (x-axis) for naïve, scV33-, and siV33-tick bites of FVB-Jax and FVB-Tac mice.

Figure 4: Impact of tick EVs on wound healing pathways through the DETC-keratinocyte axis. (A-F) Individual tSNE plots of keratinocyte clusters: **(A)** FVB-Jax, **(B)** FVB-Jax sc*V33*, **(C)** FVB-Jax si*V33*, **(D)** FVB-Tac **(E)** FVB-Tac sc*V33*, and **(F)** FVB-Tac si*V33*. **(G)** Enriched pathways in the unidentified cell cluster (as shown in **C**) based on functional annotation in DAVID. Fold enrichment is indicated in a Log2 scale. **p* value and FDR<0.05 were set as

threshold. KEGG, GO and InterPro were used as reference annotation databases. **(H)** Ingenuity pathway analysis comparing keratinocytes of skin biopsies from FVB-Jax si*V33* to FVB-Jax sc*V33*. Blue denotes pathways predicted to be inhibited (negative *z*-score) whereas orange indicates pathways predicted to be activated (positive *z*-score) based on default parameters. Differential expression datasets were assessed for canonical pathway analysis. Results are shown in a -log (*p*-value) scale. **p* value and FDR< 0.05 were set as threshold. **(I)** Volcano plot of genes representing the wound healing signaling pathway in keratinocytes of FVB-Jax si*V33* compared to FVB-Jax sc*V33* datasets (highlighted in yellow; **H**). Blue denotes decrease whereas red indicates increase in the coefficient (coef) of expression. **(J)** Dot plot of the top 5 marker genes present in the keratinocyte clusters (as shown in **A-F**). Average gene expression is demarked by the intensity of color. Percent of gene expression within individual clusters is represented by the dot diameter. **(K)** Expression of *Col1a1* on t-SNE plot of keratinocyte clusters.

Figure 5: Tick EVs impact keratinocyte proliferation. (A) Ingenuity pathway analysis derived from si*V33* compared to the bite of sc*V33* ticks on FVB-Jax or FVB-Tac mice. Canonical pathways predicted to be inhibited (blue, negative *z*-score) or activated (orange, positive *z*-score) based on differential expression profile. The solid line indicates the *p*-value significance threshold of 0.05 (-log=1.3). **(B)** The signaling cascade of EIF2 (highlighted in yellow, **A**), yielding (→) or inhibitory (⊣) arrows. Orange indicates activation whereas blue shows inhibition according to the IPA prediction. Gene expression based on the scRNAseq experiment is indicated in red (increased) or green (decreased). Gray – no expression or prediction. **(C)** Sc*V33* (circle) or si*V33* (square) injected *I. scapularis* nymphs were fed on FVB-Jax (white) or FVB-Tac (gray) mice for 3 days. Biopsies were taken from the skin at the bite site and assessed for $EpCAM^+$ $Ki67^+$ keratinocytes by flow cytometry. **(D-I)** Sc*V33* or si*V33* ticks fed on C57BL/6 mice for 3 days. Biopsies were taken from the skin at the bite site and processed for flow

cytometry analysis. **(D)** PI3K p85^{+}, and **(E)** phospho-PI3K p85/p55^{+}. **(F)** ELISA analysis of KGF normalized to total protein per 5 mm skin punch biopsy. **(G)** EpCAM^{+} Ki67^{+} keratinocytes assessed by flow cytometry. Graph displays proliferation changes within the sc*V33* or si*V33* treatments compared to the naïve skin. Data are presented as a mean with standard deviation. Statistical significance shown as *p<0.05, ns = not significant. **(C-G)** Significance was measured by One-way ANOVA followed by Tukey's *post hoc* test. **(H-I)** Flow cytometry histogram plots of EpCAM^{+} Ki67^{+} keratinocytes. **(H)** sc*V33* or **(I)** si*V33* treatments displayed according to the number of ticks bitten per biopsy. *X*-axis shows fluorescence intensity, and the *Y*-axis indicates the count of events in the fluorescence channel.

References

1. Adams, T.S. (1999). Hematophagy and hormone release. Annals of the Entomological Society of America *92*, 1-13. https://doi.org/10.1093/aesa/92.1.1.
2. Ribeiro, J.M. (1995). Blood-feeding arthropods: live syringes or invertebrate pharmacologists? Infectious Agents and Disease *4*, 143-152.
3. Sonenshine, D.E., and Roe, R.M. (2014). Biology of ticks, Second Edition (Oxford University Press).
4. Nuttall, P.A. (2019). Wonders of tick saliva. Ticks and Tick-borne diseases *10*, 470-481. 10.1016/j.ttbdis.2018.11.005.
5. Wikel, S. (2013). Ticks and tick-borne pathogens at the cutaneous interface: host defenses, tick countermeasures, and a suitable environment for pathogen establishment. Frontiers in Microbiology *4*, 337. 10.3389/fmicb.2013.00337.
6. Chmelar, J., Kotal, J., Kopecky, J., Pedra, J.H.F., and Kotsyfakis, M. (2016). All for one and one for all on the tick-host battlefield. Trends Parasitol *32*, 368-377. 10.1016/j.pt.2016.01.004.
7. Kitsou, C., Fikrig, E., and Pal, U. (2021). Tick host immunity: vector immunomodulation and acquired tick resistance. Trends Immunol *42*, 554-574. 10.1016/j.it.2021.05.005.
8. Boulanger, N., Boyer, P., Talagrand-Reboul, E., and Hansmann, Y. (2019). Ticks and tick-borne diseases. Med Mal Infect *49*, 87-97. 10.1016/j.medmal.2019.01.007.
9. Eisen, R.J., and Eisen, L. (2018). The blacklegged tick, *Ixodes scapularis*: an increasing public health concern. Trends in Parasitology *34*, 295-309. 10.1016/j.pt.2017.12.006.
10. Jongejan, F., and Uilenberg, G. (2004). The global importance of ticks. Parasitology *129 Suppl*, S3-14.
11. Rochlin, I., and Toledo, A. (2020). Emerging tick-borne pathogens of public health importance: a mini-review. J Med Microbiol *69*, 781-791. 10.1099/jmm.0.001206.
12. Bernard, Q., Grillon, A., Lenormand, C., Ehret-Sabatier, L., and Boulanger, N. (2020). Skin interface, a key player for *Borrelia* multiplication and persistence in Lyme borreliosis. Trends in Parasitology *36*, 304-314. 10.1016/j.pt.2019.12.017.
13. Kanitakis, J. (2002). Anatomy, histology and immunohistochemistry of normal human skin. Eur J Dermatol *12*, 390-399; 400-391.
14. Kabashima, K., Honda, T., Ginhoux, F., and Egawa, G. (2019). The immunological anatomy of the skin. Nat Rev Immunol *19*, 19-30. 10.1038/s41577-018-0084-5.
15. Allen, J.R., Khalil, H.M., and Wikel, S.K. (1979). Langerhans cells trap tick salivary gland antigens in tick-resistant guinea pigs. Journal of Immunology *122*, 563-565.
16. Oliva Chavez, A.S., Wang, X., Marnin, L., Archer, N.K., Hammond, H.L., Carroll, E.E.M., Shaw, D.K., Tully, B.G., Buskirk, A.D., Ford, S.L., et al. (2021). Tick extracellular vesicles enable arthropod feeding and promote distinct outcomes of bacterial infection. Nature Communications *12*, 3696. 10.1038/s41467-021-23900-8.
17. Heilig, J.S., and Tonegawa, S. (1986). Diversity of murine gamma genes and expression in fetal and adult T lymphocytes. Nature *322*, 836-840. 10.1038/322836a0.
18. Garman, R.D., Doherty, P.J., and Raulet, D.H. (1986). Diversity, rearrangement, and expression of murine T cell gamma genes. Cell *45*, 733-742. 10.1016/0092-8674(86)90787-7.
19. Suter, M.M., Schulze, K., Bergman, W., Welle, M., Roosje, P., and Muller, E.J. (2009). The keratinocyte in epidermal renewal and defence. Vet Dermatol *20*, 515-532. 10.1111/j.1365-3164.2009.00819.x.
20. Suter, M.M., Crameri, F.M., Olivry, T., Mueller, E., Tscharner, C.V., and Jensen, P.J. (1997). Keratinocyte biology and pathology. Vet Dermatol *8*, 67-100. 10.1046/j.1365-3164.1997.d01-5.x.
21. Piipponen, M., Li, D., and Landen, N.X. (2020). The immune functions of keratinocytes in skin wound healing. Int J Mol Sci *21,* 8790. 10.3390/ijms21228790.

22. Nestle, F.O., Di Meglio, P., Qin, J.Z., and Nickoloff, B.J. (2009). Skin immune sentinels in health and disease. Nat Rev Immunol *9*, 679-691. 10.1038/nri2622.
23. Sharp, L.L., Jameson, J.M., Cauvi, G., and Havran, W.L. (2005). Dendritic epidermal T cells regulate skin homeostasis through local production of insulin-like growth factor 1. Nature Immunology *6*, 73-79. 10.1038/ni1152.
24. Boismenu, R., and Havran, W.L. (1994). Modulation of epithelial cell growth by intraepithelial γδ T cells. Science *266*, 1253-1255. 10.1126/science.7973709.
25. Boismenu, R., Feng, L., Xia, Y.Y., Chang, J.C., and Havran, W.L. (1996). Chemokine expression by intraepithelial γδ T cells. Implications for the recruitment of inflammatory cells to damaged epithelia. Journal of Immunology *157*, 985-992.
26. Jameson, J., and Havran, W.L. (2007). Skin γδ T-cell functions in homeostasis and wound healing. Immunological Reviews *215*, 114-122. 10.1111/j.1600-065X.2006.00483.x.
27. Jameson, J., Ugarte, K., Chen, N., Yachi, P., Fuchs, E., Boismenu, R., and Havran, W.L. (2002). A role for skin γδ T cells in wound repair. Science *296*, 747-749. 10.1126/science.1069639.
28. Sharma, A., Pham, M.N., Reyes, J.B., Chana, R., Yim, W.C., Heu, C.C., Kim, D., Chaverra-Rodriguez, D., Rasgon, J.L., Harrell, R.A., 2nd, et al. (2022). Cas9-mediated gene editing in the black-legged tick, *Ixodes scapularis*, by embryo injection and ReMOT Control. iScience *25*, 103781. 10.1016/j.isci.2022.103781.
29. Havran, W.L., Chien, Y.H., and Allison, J.P. (1991). Recognition of self antigens by skin-derived T cells with invariant γδ antigen receptors. Science *252*, 1430-1432. 10.1126/science.1828619.
30. Witherden, D.A., Verdino, P., Rieder, S.E., Garijo, O., Mills, R.E., Teyton, L., Fischer, W.H., Wilson, I.A., and Havran, W.L. (2010). The junctional adhesion molecule JAML is a costimulatory receptor for epithelial γδ T cell activation. Science *329*, 1205-1210. 10.1126/science.1192698.
31. Witherden, D.A., Watanabe, M., Garijo, O., Rieder, S.E., Sarkisyan, G., Cronin, S.J., Verdino, P., Wilson, I.A., Kumanogoh, A., Kikutani, H., et al. (2012). The CD100 receptor interacts with its plexin B2 ligand to regulate epidermal γδ T cell function. Immunity *37*, 314-325. 10.1016/j.immuni.2012.05.026.
32. Yoshida, S., Mohamed, R.H., Kajikawa, M., Koizumi, J., Tanaka, M., Fugo, K., Otsuka, N., Maenaka, K., Yagita, H., Chiba, H., and Kasahara, M. (2012). Involvement of an NKG2D ligand H60c in epidermal dendritic T cell-mediated wound repair. J Immunol *188*, 3972-3979. 10.4049/jimmunol.1102886.
33. Nielsen, M.M., Witherden, D.A., and Havran, W.L. (2017). γδ T cells in homeostasis and host defence of epithelial barrier tissues. Nat Rev Immunol *17*, 733-745. 10.1038/nri.2017.101.
34. Park, S., Matte-Martone, C., Gonzalez, D.G., Lathrop, E.A., May, D.P., Pineda, C.M., Moore, J.L., Boucher, J.D., Marsh, E., Schmitter-Sanchez, A., et al. (2021). Skin-resident immune cells actively coordinate their distribution with epidermal cells during homeostasis. Nature Cell Biology *23*, 476-484. 10.1038/s41556-021-00670-5.
35. Havran, W.L., and Jameson, J.M. (2010). Epidermal T cells and wound healing. Journal of Immunology *184*, 5423-5428. 10.4049/jimmunol.0902733.
36. Lewis, J.M., Girardi, M., Roberts, S.J., Barbee, S.D., Hayday, A.C., and Tigelaar, R.E. (2006). Selection of the cutaneous intraepithelial $\gamma\delta^+$ T cell repertoire by a thymic stromal determinant. Nature Immunology *7*, 843-850. 10.1038/ni1363.
37. Boyden, L.M., Lewis, J.M., Barbee, S.D., Bas, A., Girardi, M., Hayday, A.C., Tigelaar, R.E., and Lifton, R.P. (2008). Skint1, the prototype of a newly identified immunoglobulin

superfamily gene cluster, positively selects epidermal gammadelta T cells. Nature Genetics *40*, 656-662. 10.1038/ng.108.

38. Barbee, S.D., Woodward, M.J., Turchinovich, G., Mention, J.J., Lewis, J.M., Boyden, L.M., Lifton, R.P., Tigelaar, R., and Hayday, A.C. (2011). Skint-1 is a highly specific, unique selecting component for epidermal T cells. Proceedings of the National Academy of Sciences of the United States of America *108*, 3330-3335. 10.1073/pnas.1010890108.
39. Joost, S., Zeisel, A., Jacob, T., Sun, X., La Manno, G., Lonnerberg, P., Linnarsson, S., and Kasper, M. (2016). Single-cell transcriptomics reveals that differentiation and spatial signatures shape epidermal and hair follicle heterogeneity. Cell Syst *3*, 221-237 e229. 10.1016/j.cels.2016.08.010.
40. Joost, S., Jacob, T., Sun, X., Annusver, K., La Manno, G., Sur, I., and Kasper, M. (2018). Single-cell transcriptomics of traced epidermal and hair follicle stem cells reveals rapid adaptations during wound healing. Cell Reports *25*, 585-597 e587. 10.1016/j.celrep.2018.09.059.
41. Keyes, B.E., Liu, S., Asare, A., Naik, S., Levorse, J., Polak, L., Lu, C.P., Nikolova, M., Pasolli, H.A., and Fuchs, E. (2016). Impaired epidermal to dendritic T cell signaling slows wound repair in aged skin. Cell *167*, 1323-1338 e1314. 10.1016/j.cell.2016.10.052.
42. Saelens, W., Cannoodt, R., Todorov, H., and Saeys, Y. (2019). A comparison of single-cell trajectory inference methods. Nat Biotechnol *37*, 547-554. 10.1038/s41587-019-0071-9.
43. Fuchs, E. (1990). Epidermal differentiation: the bare essentials. J Cell Biol *111*, 2807-2814. 10.1083/jcb.111.6.2807.
44. Misiura, M., Baszanowska, W., Oscilowska, I., Palka, J., and Miltyk, W. (2020). Prolidase stimulates proliferation and migration through activation of the PI3K/Akt/mTOR signaling pathway in human keratinocytes. Int J Mol Sci *21*. 10.3390/ijms21239243.
45. Bartolo, I., Reis, R.L., Marques, A.P., and Cerqueira, M.T. (2022). Keratinocyte growth factor-based strategies for wound re-epithelialization. Tissue Eng Part B Rev *28*, 665-676. 10.1089/ten.TEB.2021.0030.
46. Matsuura-Hachiya, Y., Arai, K.Y., Muraguchi, T., Sasaki, T., and Nishiyama, T. (2018). Type IV collagen aggregates promote keratinocyte proliferation and formation of epidermal layer in human skin equivalents. Exp Dermatol *27*, 443-448. 10.1111/exd.13328.
47. Angel, P., Szabowski, A., and Schorpp-Kistner, M. (2001). Function and regulation of AP-1 subunits in skin physiology and pathology. Oncogene *20*, 2413-2423. 10.1038/sj.onc.1204380.
48. Li, G., Gustafson-Brown, C., Hanks, S.K., Nason, K., Arbeit, J.M., Pogliano, K., Wisdom, R.M., and Johnson, R.S. (2003). c-Jun is essential for organization of the epidermal leading edge. Dev Cell *4*, 865-877. 10.1016/s1534-5807(03)00159-x.
49. Calautti, E., Li, J., Saoncella, S., Brissette, J.L., and Goetinck, P.F. (2005). Phosphoinositide 3-kinase signaling to Akt promotes keratinocyte differentiation versus death. J Biol Chem *280*, 32856-32865. 10.1074/jbc.M506119200.
50. Castilho, R.M., Squarize, C.H., and Gutkind, J.S. (2013). Exploiting PI3K/mTOR signaling to accelerate epithelial wound healing. Oral Dis *19*, 551-558. 10.1111/odi.12070.
51. Tanner, S.M., and Lorenz, R.G. (2022). FVB/N mouse strain regulatory T cells differ in phenotype and function from the C57BL/6 and BALB/C strains. FASEB Bioadv *4*, 648-661. 10.1096/fba.2021-00161.
52. Woodworth, C.D., Michael, E., Smith, L., Vijayachandra, K., Glick, A., Hennings, H., and Yuspa, S.H. (2004). Strain-dependent differences in malignant conversion of mouse skin tumors is an inherent property of the epidermal keratinocyte. Carcinogenesis *25*, 1771-1778. 10.1093/carcin/bgh170.

53. Jameson, J.M., Cauvi, G., Witherden, D.A., and Havran, W.L. (2004). A keratinocyte-responsive γδ TCR is necessary for dendritic epidermal T cell activation by damaged keratinocytes and maintenance in the epidermis. Journal of Immunology *172*, 3573-3579. 10.4049/jimmunol.172.6.3573.
54. Hayday, A.C., and Vantourout, P. (2020). The innate biologies of adaptive antigen receptors. Annual Review of Immunology *38*, 487-510. 10.1146/annurev-immunol-102819-023144.
55. Toulon, A., Breton, L., Taylor, K.R., Tenenhaus, M., Bhavsar, D., Lanigan, C., Rudolph, R., Jameson, J., and Havran, W.L. (2009). A role for human skin-resident T cells in wound healing. The Journal of Experimental Medicine *206*, 743-750. 10.1084/jem.20081787.
56. Strobl, J., Mundler, V., Muller, S., Gindl, A., Berent, S., Schotta, A.M., Kleissl, L., Staud, C., Redl, A., Unterluggauer, L., et al. (2022). Tick feeding modulates the human skin immune landscape to facilitate tick-borne pathogen transmission. J Clin Invest *132*, e161188. 10.1172/JCI161188.
57. Dekoninck, S., and Blanpain, C. (2019). Stem cell dynamics, migration and plasticity during wound healing. Nature Cell Biology *21*, 18-24. 10.1038/s41556-018-0237-6.
58. Jochum, W., Passegue, E., and Wagner, E.F. (2001). AP-1 in mouse development and tumorigenesis. Oncogene *20*, 2401-2412. 10.1038/sj.onc.1204389.
59. Aragona, M., Dekoninck, S., Rulands, S., Lenglez, S., Mascre, G., Simons, B.D., and Blanpain, C. (2017). Defining stem cell dynamics and migration during wound healing in mouse skin epidermis. Nature Communications *8*, 14684. 10.1038/ncomms14684.
60. Park, S., Gonzalez, D.G., Guirao, B., Boucher, J.D., Cockburn, K., Marsh, E.D., Mesa, K.R., Brown, S., Rompolas, P., Haberman, A.M., et al. (2017). Tissue-scale coordination of cellular behaviour promotes epidermal wound repair in live mice. Nature Cell Biology *19*, 155-163. 10.1038/ncb3472.
61. Ni, X., and Lai, Y. (2020). Keratinocyte: A trigger or an executor of psoriasis? J Leukoc Biol *108*, 485-491. 10.1002/JLB.5MR0120-439R.
62. Hajnicka, V., Vancova-Stibraniova, I., Slovak, M., Kocakova, P., and Nuttall, P.A. (2011). Ixodid tick salivary gland products target host wound healing growth factors. International Journal for Parasitology *41*, 213-223. 10.1016/j.ijpara.2010.09.005.
63. Leal-Galvan, B., Harvey, C., Thomas, D., Saelao, P., and Chavez, A.S.O. (2022). Isolation of microRNAs from tick *ex vivo* salivary gland cultures and extracellular vesicles. JoVE, e63618. doi:10.3791/63618.
64. Schoeler, G.B., Manweiler, S.A., and Wikel, S.K. (1999). *Ixodes scapularis*: effects of repeated infestations with pathogen-free nymphs on macrophage and T lymphocyte cytokine responses of BALB/c and C3H/HeN mice. Experimental Parasitology *92*, 239-248. 10.1006/expr.1999.4426.
65. Lun, A.T., McCarthy, D.J., and Marioni, J.C. (2016). A step-by-step workflow for low-level analysis of single-cell RNA-seq data with Bioconductor. F1000Res *5*, 2122. 10.12688/f1000research.9501.2.
66. Lun, A.T., Bach, K., and Marioni, J.C. (2016). Pooling across cells to normalize single-cell RNA sequencing data with many zero counts. Genome Biology *17*, 75. 10.1186/s13059-016-0947-7.
67. McGinnis, C.S., Murrow, L.M., and Gartner, Z.J. (2019). DoubletFinder: doublet detection in single-cell RNA sequencing data using artificial nearest neighbors. Cell Syst *8*, 329-337 e324. 10.1016/j.cels.2019.03.003.
68. Street, K., Risso, D., Fletcher, R.B., Das, D., Ngai, J., Yosef, N., Purdom, E., and Dudoit, S. (2018). Slingshot: cell lineage and pseudotime inference for single-cell transcriptomics. BMC Genomics *19*, 477. 10.1186/s12864-018-4772-0.

69. Finak, G., McDavid, A., Yajima, M., Deng, J., Gersuk, V., Shalek, A.K., Slichter, C.K., Miller, H.W., McElrath, M.J., Prlic, M., et al. (2015). MAST: a flexible statistical framework for assessing transcriptional changes and characterizing heterogeneity in single-cell RNA sequencing data. Genome Biol *16*, 278. 10.1186/s13059-015-0844-5.
70. Calvano, S.E., Xiao, W., Richards, D.R., Felciano, R.M., Baker, H.V., Cho, R.J., Chen, R.O., Brownstein, B.H., Cobb, J.P., Tschoeke, S.K., et al. (2005). A network-based analysis of systemic inflammation in humans. Nature *437*, 1032-1037. 10.1038/nature03985.

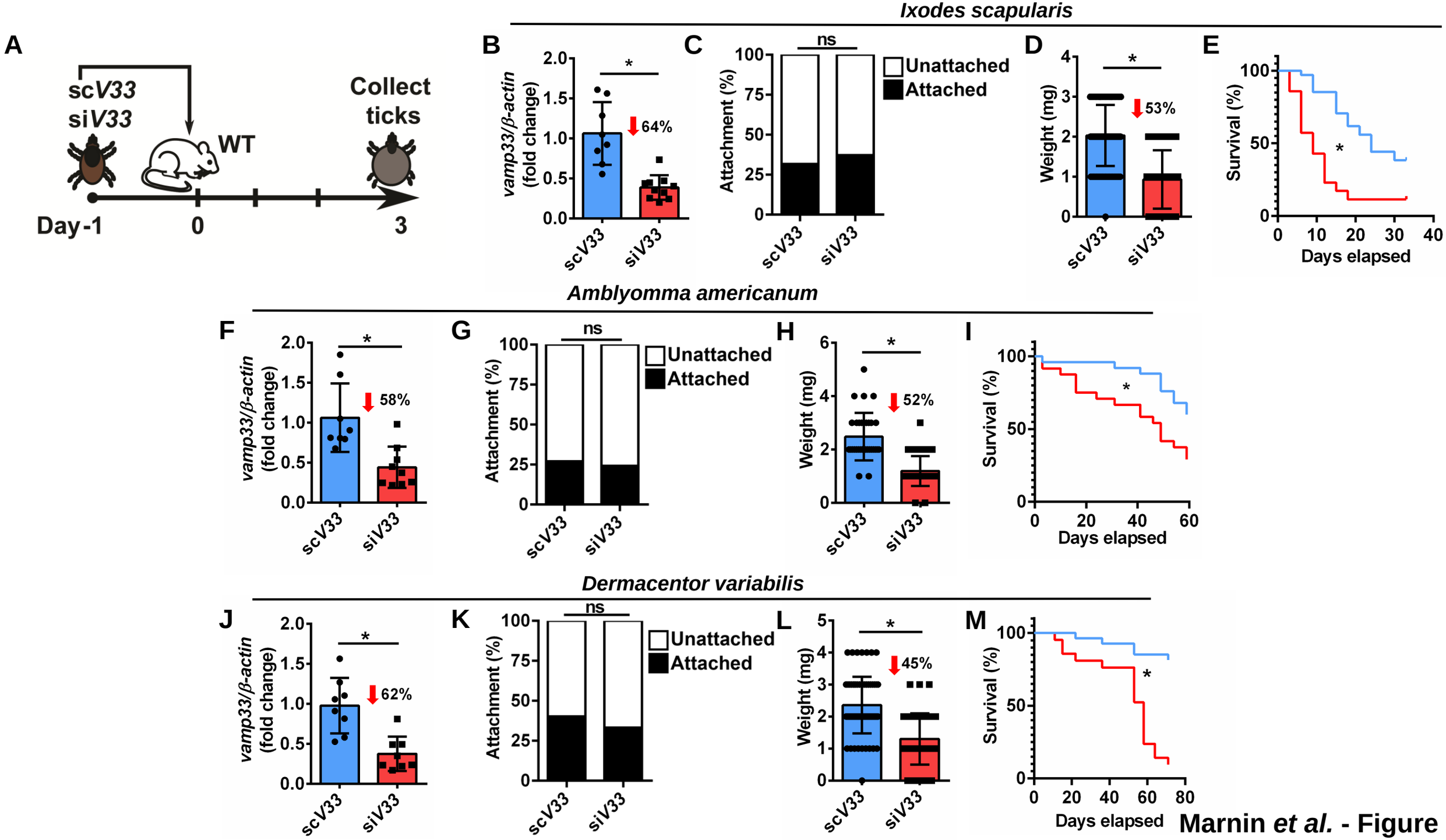
Ixodes scapularis
A
scV33
siV33
WT
Collect ticks
Day-1
0
3
B
vamp33/β-actin (fold change)
64%
scV33
siV33
C
ns
Attachment (%)
Unattached
Attached
D
Weight (mg)
53%
E
Survival (%)
Days elapsed
Amblyomma americanum
F
58%
G
H
52%
I
Dermacentor variabilis
J
62%
K
L
45%
M
Marnin et al. - Figure 1

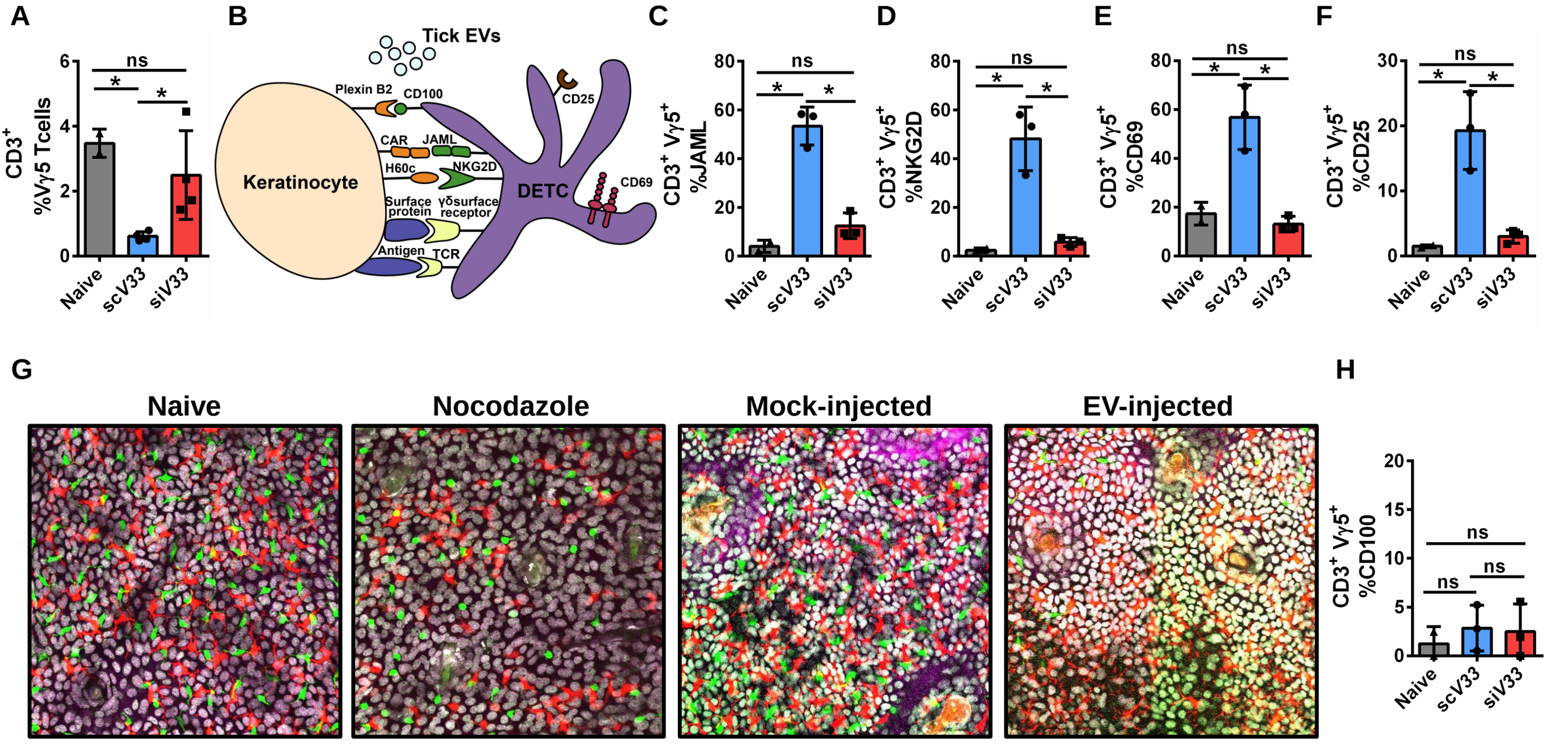

Marnin *et al.* - Figure 2

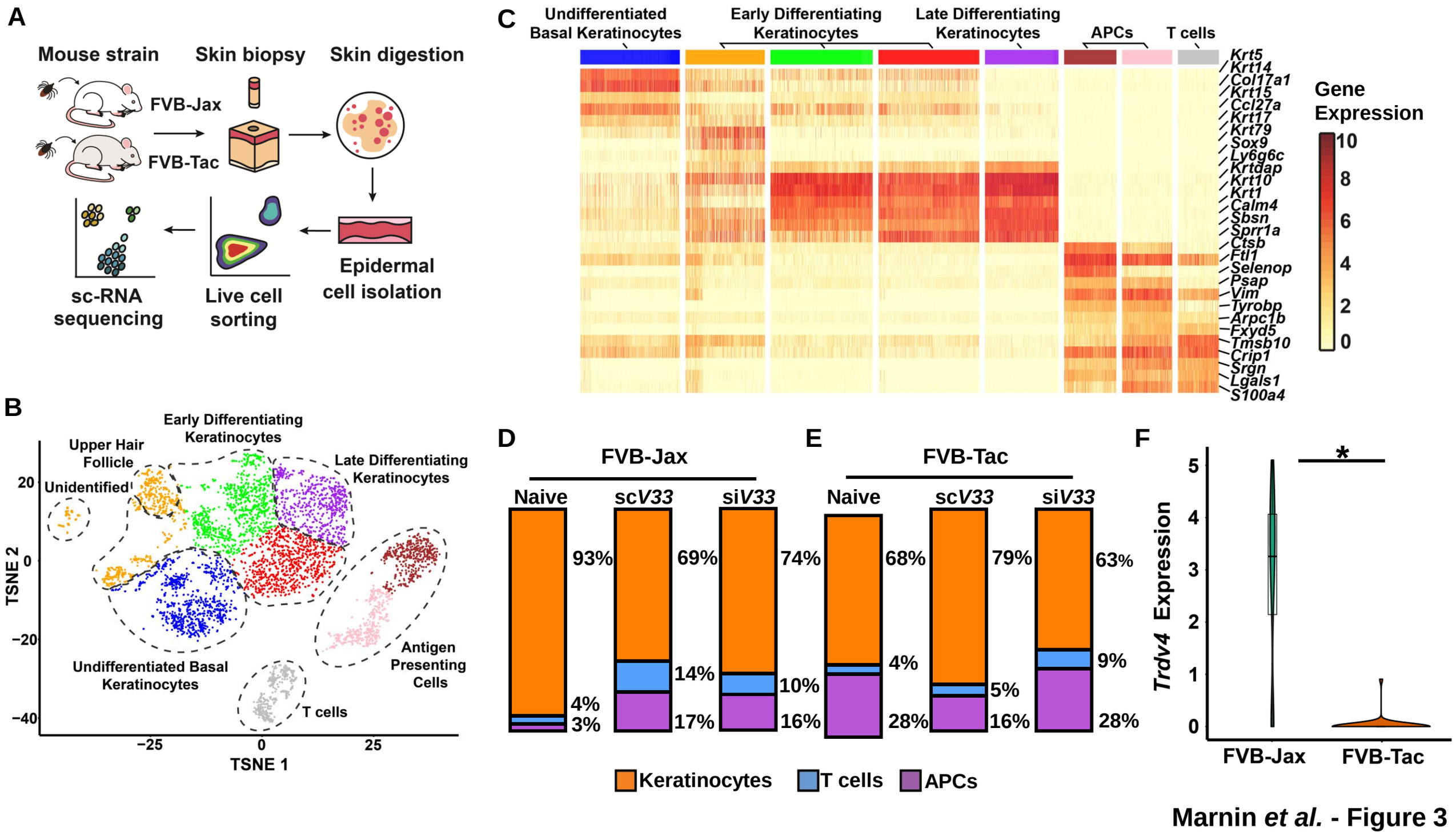

Marnin *et al.* - Figure 3

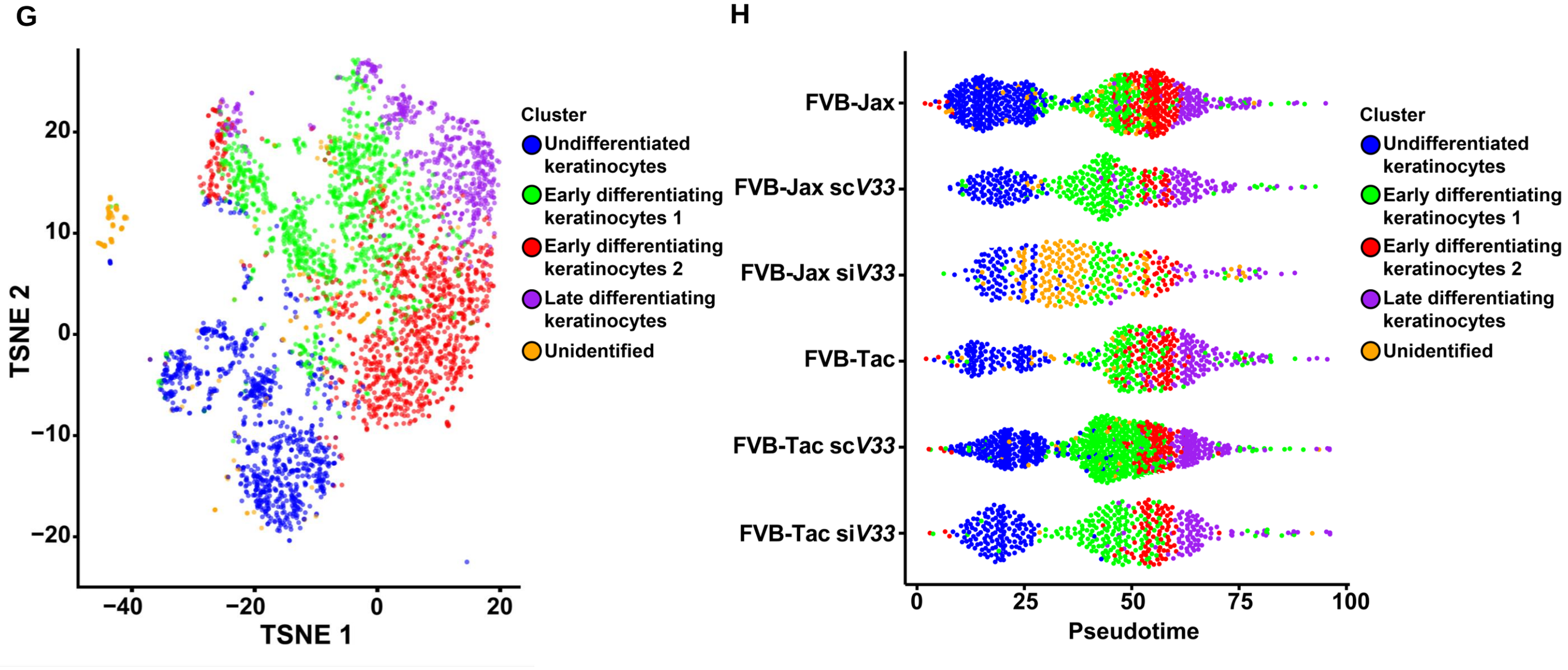

Marnin *et al.* - Figure 3 (continued)

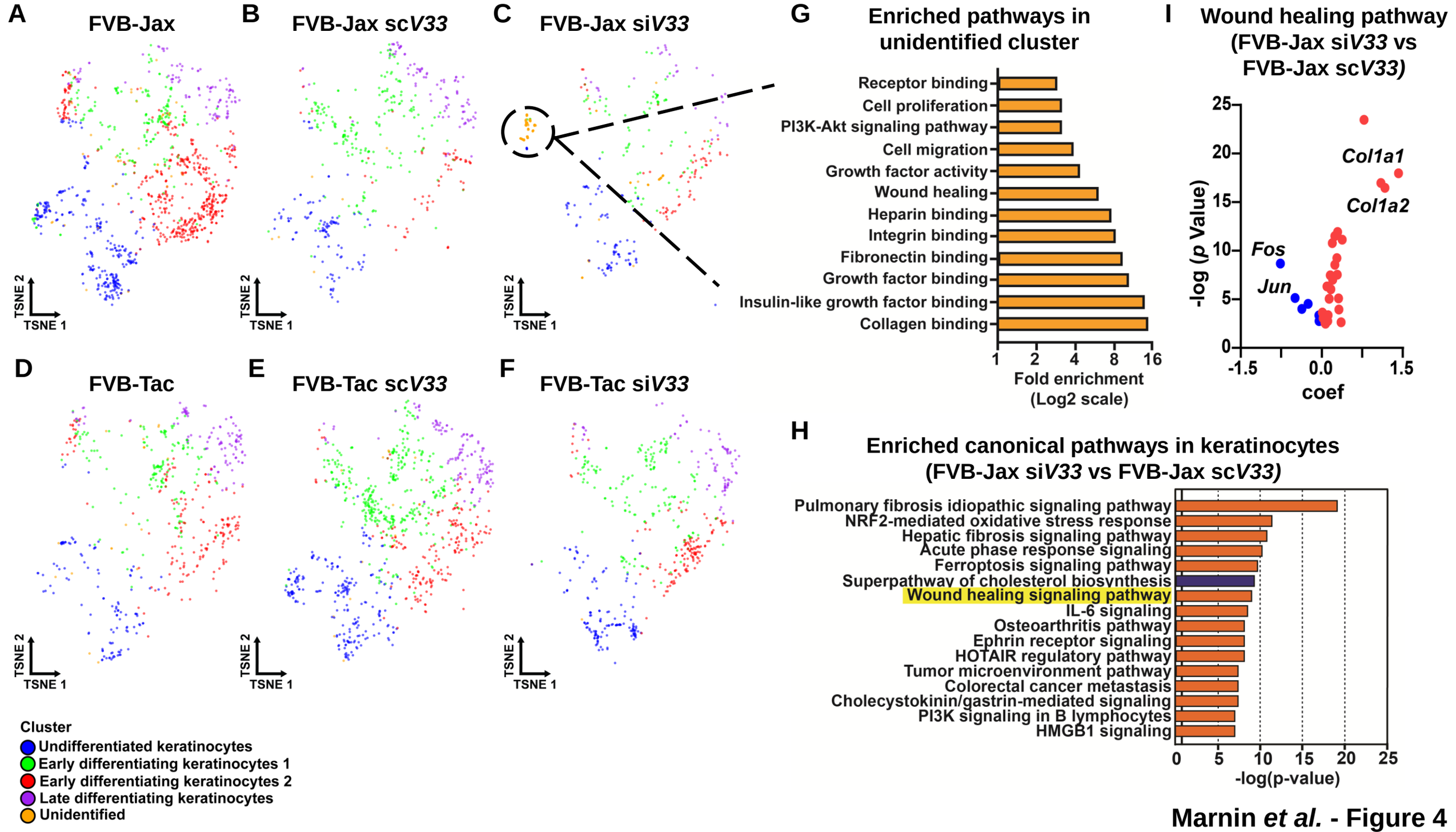

Marnin *et al.* - Figure 4

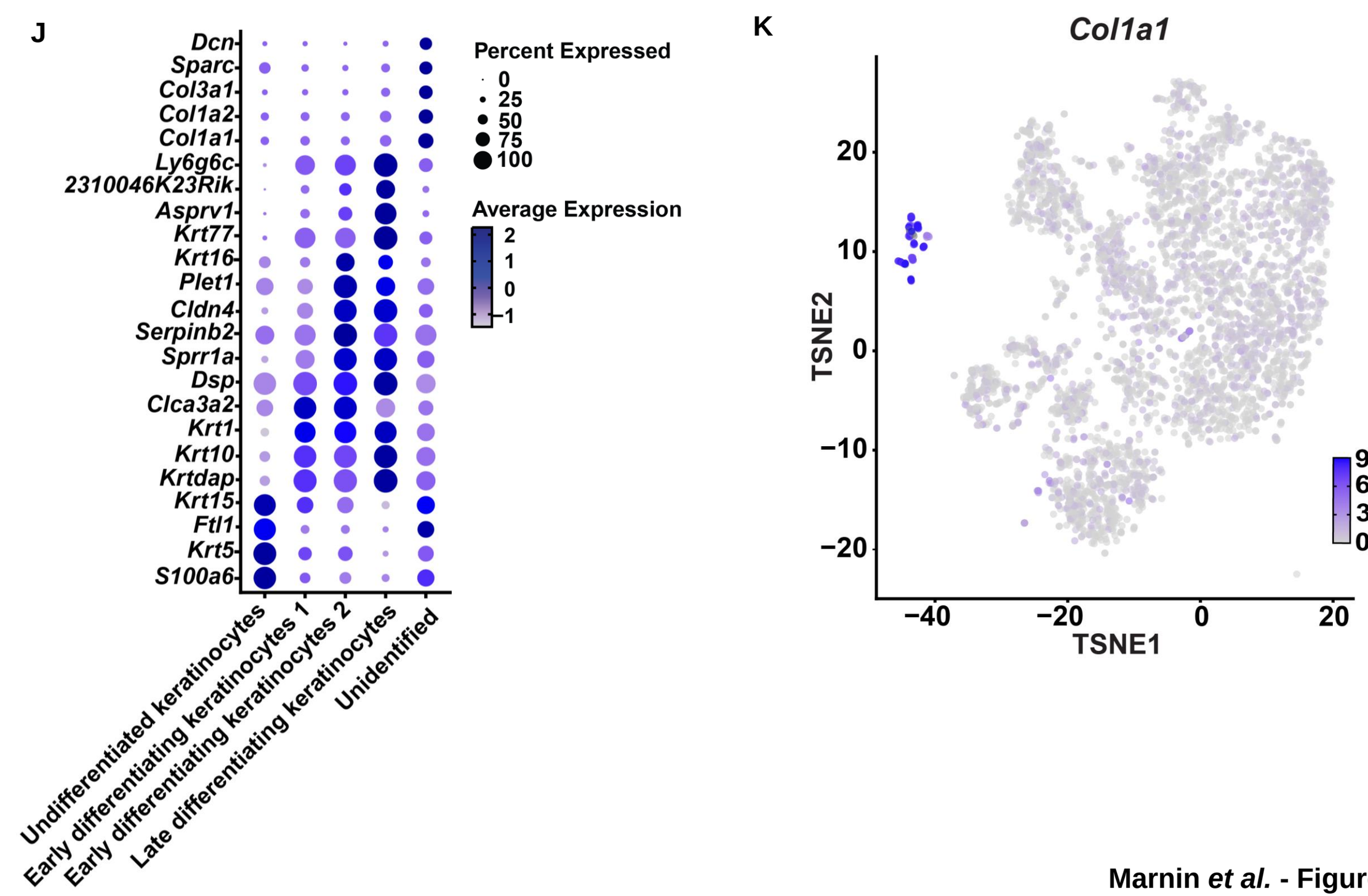

Marnin *et al.* - Figure 4 (continued)

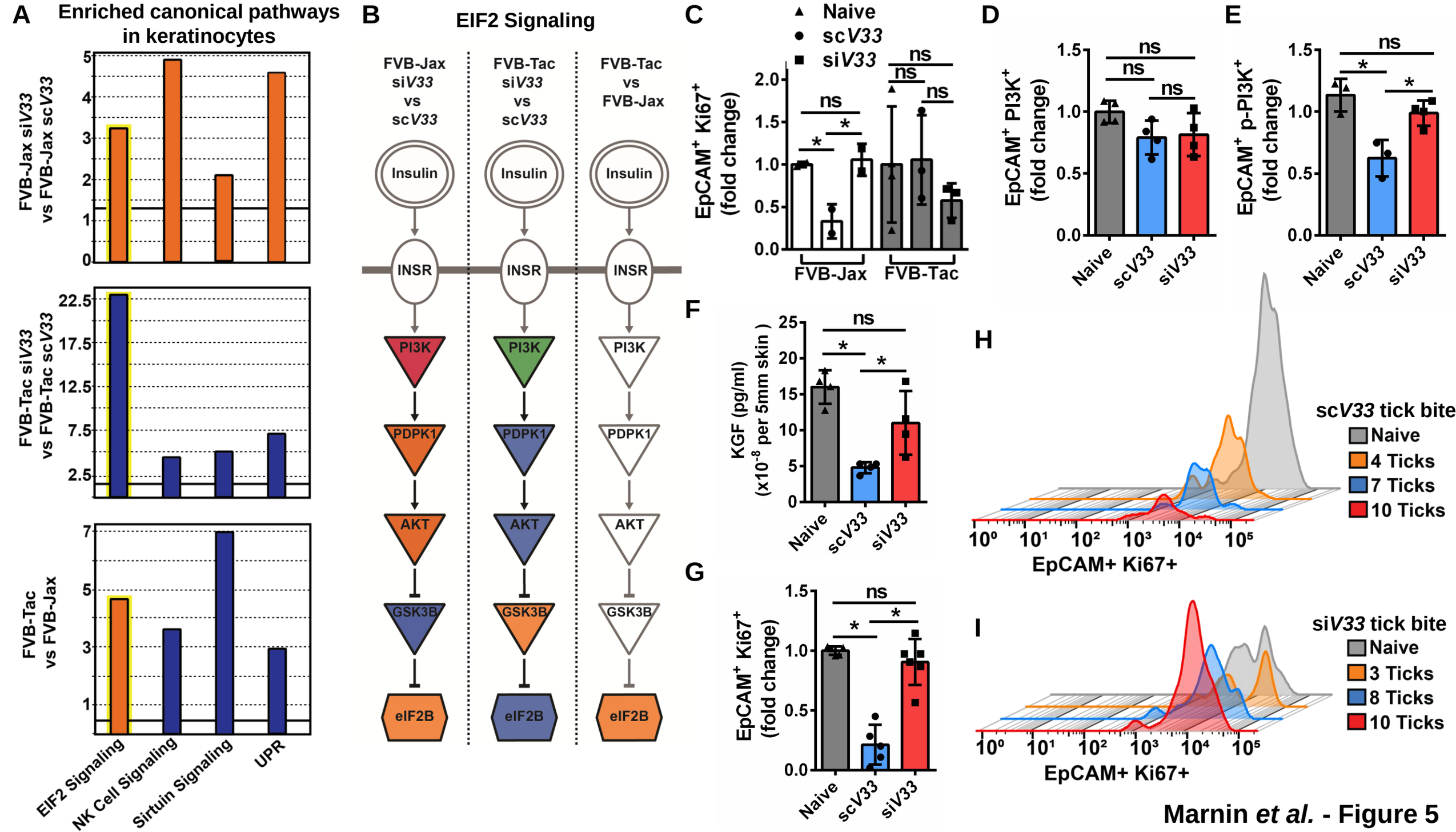
A
Enriched canonical pathways in keratinocytes
FVB-Jax siV33 vs FVB-Jax scV33
FVB-Tac siV33 vs FVB-Tac scV33
FVB-Tac vs FVB-Jax
EIF2 Signaling
NK Cell Signaling
Sirtuin Signaling
UPR
B
EIF2 Signaling
FVB-Jax siV33 vs scV33
FVB-Tac siV33 vs scV33
FVB-Tac vs FVB-Jax
Insulin
INSR
PI3K
PDPK1
AKT
GSK3B
eIF2B
C
Naive
scV33
siV33
EpCAM+ Ki67+ (fold change)
FVB-Jax
FVB-Tac
D
EpCAM+ PI3K+ (fold change)
E
EpCAM+ p-PI3K+ (fold change)
F
KGF (pg/ml) (x10-8 per 5mm skin)
G
EpCAM+ Ki67+ (fold change)
H
scV33 tick bite
Naive
4 Ticks
7 Ticks
10 Ticks
EpCAM+ Ki67+
I
siV33 tick bite
Naive
3 Ticks
8 Ticks
10 Ticks
EpCAM+ Ki67+
ns
Marnin et al. - Figure 5